Nucleation control and interface structure of rocksalt PbSe on (001) zincblende III-V surfaces

Brian B. Haidet, Eamonn T. Hughes, and Kunal Mukherjee*
Materials Department, University of California Santa Barbara, Santa Barbara, California 93106, USA

(Received 5 September 2019; accepted 7 February 2020; published 4 March 2020)

We study the early stages of growth of the IV-VI semiconductor PbSe on (001)-oriented III-V substrates with different surface chemistry and lattice parameter, with the aim of achieving high quality cube-on-cube rocksalt on zincblende epitaxy. We find that PbSe nucleation on bare GaSb, InAs, and GaAs substrates is varied, yet consistently results in mixed orientation growth due to chemistry-dependent interfacial-energy penalties, irrespective of lattice mismatch. To overcome this, we locate a growth window for cube-on-cube single-orientation nucleation of PbSe on III-arsenide surfaces utilizing a high-temperature surface treatment with PbSe flux that we find creates a better template for subsequent low-temperature growth and leads to sharp interfaces. We probe this interface between PbSe and InAs, finding a Chain[Pb,As] atomic arrangement, tantamount to a discontinuous anion sublattice between III-V and IV-VI materials. We also observe a vertical displacement of the first few monolayers of the Se sublattice that we believe has origins in the heterovalency of this interface. Our results point towards surface chemistry as the primary factor governing film orientation, and lattice mismatch governing island coalescence behavior in these heterovalent interfaces with dissimilar crystal structures.

DOI: 10.1103/PhysRevMaterials.4.033402

I. INTRODUCTION

Heteroepitaxy of materials involving the growth of dissimilar crystals results in nontrivial interface atomic arrangements, unexpected film-substrate orientation relationships, and overall complex growth mechanisms [1]. Yet, the ability to control such interfaces holds the key to different phenomena and device designs, harnessing features of both materials and potentially leading to emergent properties. Systematic studies in the heteroepitaxy of heterovalent semiconductors with isocrystal structures (e.g., GaAs/Ge, ZnSe/GaAs, etc.) have yielded methods to tune otherwise immutable electronic properties like the band alignment [2]. Likewise, control over isovalent interfaces with different crystal structures such as that in ErAs/GaAs have resulted in advances in the fields of optoelectronics and thermoelectrics [3–5]. In this work, we expand on these pioneering efforts by exploring tools to mediate both heterovalency and heterocrystal structures in semiconductors. For this, we explore the epitaxial growth of the mixed covalent-ionic rocksalt IV-VI semiconductor family, specifically PbSe, on covalent zincblende III-V substrates. This system presents an opportunity to study such growth phenomena towards marrying these two classes of materials.

Understanding these complex interfaces holds the key to engineering IV-VI-based mid-infrared (mid-IR) optoelectronic devices [6–12] as well as harnessing the properties of recently discovered topologically nontrivial states [13–19]. Specifically, midinfrared light emitters and detectors based on narrow-gap IV-VI materials could benefit significantly from high-quality nearly lattice-matched III-V substrates, as native IV-VI substrates are fragile, poor dissipaters of heat, and limited in quality and availability. To this end, we note that PbSe/GaSb heterostructures have been proposed [20] for mid-IR lasers, although only one study [21] on PbSe/GaSb growth has been reported, the latter using liquid phase epitaxy (LPE) to synthesize PbSe quantum dots on GaSb. Controlling the atypical heterovalent interface atomic arrangement between these materials will also grant control over the induced interfacial charge, with both electronic and structural implications for thin films. In addition to classical optoelectronics, a subclass of IV-VI materials including PbSnSe and PbSnTe belong to the topological crystalline insulator phase of matter, and these heterointerfaces can host electronic states. The ability to grow ordered interfaces between topologically trivial and nontrivial materials would expand the study of the well-known nontrivial surface states to interface states [22] that have the potential to be pristine and controllable.

The unique mix of ionic, covalent, and metallic bonding [23] in IV-VI materials has historically made them difficult to integrate with other semiconductors. The cubic PbSe and PbSnSe phases form the rocksalt crystal structure with sixfold coordination based on a set of resonant *p*-like orbitals oriented at 90° to each other [24]. III-V materials, on the other hand, have fourfold coordination based on *sp*3 hybridized orbitals that form bond angles of 109.5°. Any interface between these materials will necessarily have a layer of disordered bonding and coordination. This disorder creates significant interfacial energy penalties for epitaxy and diminishes the possibility for layer-by-layer growth. As a majority of the work on IV-VI semiconductors has utilized fluorite substrates or buffers of CaF_2 and BaF_2, literature on the early stages of growth of IV-VI materials on III-V substrates is limited [21,25–27]. On (001) GaAs, PbTe has been observed to grow in mixtures of (001) and (111) orientations [26,27]. On tellurium-treated GaAs [25] there are reports of cube-on-cube (001)-oriented

*kunalm@ucsb.edu

PbSe growth. However, on (211) GaAs [25], (211) ZnTe [28], and (001) GaSb [21], PbSe does not grow cube-on cube but instead misnucleates in either the (511) or (110) orientations. On (111) Si substrates, the nucleation orientation of PbSe depends on temperature [29]. While on CaF_2, PbTe orientation is based on step orientation and varies with surface/subsurface defects [30]. The most common substrate for IV-VI growth is (111)-oriented BaF_2, where nuclei orientation seems to be less of a problem, but very weak interaction between the film and substrate leads to low sticking coefficients, large islands, and slow coalescence [31–33]. Overall, epitaxy of the rocksalt IV-VIs seems to be dominated by high interfacial energies and weak bonding between the film and substrate.

In this study, we locate growth windows for single-orientation nucleation of (001) PbSe by molecular beam epitaxy (MBE) and examine the interfacial atomic arrangement to learn about the transition in bonding from III-V to IV-VI. On bare (001) III-V substrates GaSb, InAs, and GaAs, with 0.5%, 1.1%, and 7.7% mismatch to PbSe at room temperature, respectively, we find no satisfactory growth windows—mixtures of misoriented nuclei are observed with areal ratios that depend on the substrate temperature. However, we do find a high-temperature surface treatment with PbSe flux is effective in controlling nucleation on InAs and GaAs (but not GaSb) substrates and results in reliable cube-on-cube epitaxial arrangement of PbSe. Using high-resolution scanning transmission electron microscopy (HR-STEM), we find that this treatment leads to a sharp PbSe-InAs heterointerface. As the anion sublattice breaks continuity between the two crystal structures, it appears the lead atoms assume most of the necessary bonding disorder. Overall, these results highlight the importance of both the starting chemistry of the surfaces as well as growth chemistry when working with dissimilar materials, pointing the way to the creation of heterostructures of IV-VI and III-V materials.

II. MIXED-ORIENTATION PbSe NUCLEATION ON BARE III-V SURFACES

The dynamic nature of the film during nucleation and coalescence makes the early stages of growth extremely important to eventual film quality, but this period is also the most difficult to observe. Reflection high-energy electron diffraction (RHEED) was our primary characterization technique to assess the orientation and growth mode of PbSe nuclei *in situ*, during and after nucleation. We first examine PbSe nucleation on bare III-V surfaces. We observe similar behavior on (001) GaSb, InAs, and GaAs, but the detail shown here will focus on bare GaSb surfaces as a prototypical III-V bulk material with the lowest lattice-constant mismatch to PbSe.

Figures 1(a) and 1(b) shows $[1\bar{1}0]$ RHEED patterns during PbSe growth on 3×1 reconstructed (001) GaSb at high and low growth temperatures. These substrate temperatures correspond to distinct nucleation regimes that we corroborate via scanning electron microscopy (SEM). Figure 1(a) shows the case when substrate temperature is high, above ≈340 °C, and the RHEED pattern observed is a superposition of three indexable patterns [Figs. 1(c) and 1(d)], which correspond to a mix of (001)-, (221)-, and $(22\bar{1})$-oriented PbSe nuclei. The spots corresponding to (001)-oriented nuclei are also slightly more elongated vertically, indicating flatter islands. A different nuclei orientation prevails at growth temperatures below ≈300 °C. This can be seen in the pattern in Fig. 1(b)

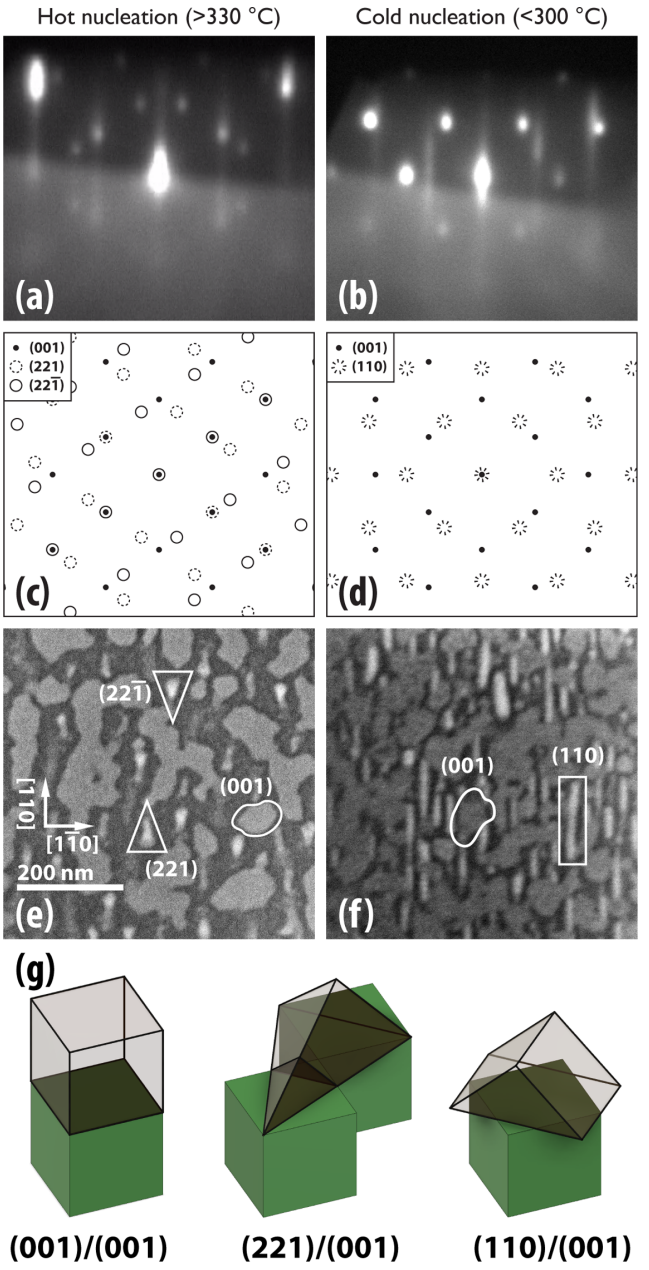

FIG. 1. PbSe nucleation on GaSb: (a),(b), $[1\bar{1}0]$ RHEED patterns of PbSe nucleated above 330 °C and PbSe nucleated below 300 °C. (b),(c) calculated RHEED patterns corresponding to different nuclei orientations. (e),(f) SEM micrographs of 90-s [∼15 monolayers (ML)] growths of PbSe on GaSb, showing (e) a mix of (001), (221), and $(22\bar{1})$ nuclei, and (f) a mix of (001) and (110) nuclei. The flat tops of the (001) nuclei and the 3D nature of the misoriented nuclei is also reflected in the shape of the observed diffraction spots—the (001) spots appear vertically stretched while the diffraction spots of off-orientation nuclei are sharper points. (g) Shows schematics of the relevant (001)-terminated nuclei shapes for a lattice-matched film. The (221) orientation actually provides perfect lattice matching with a short-range coincident site lattice. The (110) nuclei are heavily mismatched and likely strained during deposition.

showing a superposition of two diffraction patterns from a mix of (001)- and (110)-oriented nuclei. At intermediate temperatures, all four orientations of nuclei could be observed in a single growth.

From the corresponding SEM images in Figs. 1(e) and 1(f), we can see that the PbSe island shape appears to be governed by the low-energy {100} rocksalt surfaces: (001)-oriented nuclei are large and have flat (001) tops; while (221)- and (22$\bar{1}$)-oriented nuclei form opposing triangular pyramids. (110)-oriented nuclei observed at lower substrate temperatures form long tent-like structures on the surface Figs. 1(e)–1(g).

From analogous experiments, we see that PbSe islands also nucleate with multiple orientations on 2×5 Sb-terminated GaSb surfaces, Ga-terminated GaSb surfaces, and 4×2 and 2×4 As-terminated surfaces of InAs and GaAs, respectively. Nevertheless, the highly faceted nature of the PbSe islands leads to single-orientation films eventually via overgrowth. With continued deposition (typically 20–40 nm), the (001)-oriented nuclei outgrow the other orientations due to geometric factors—as seen in Figs. 1(e)–1(g), the low-energy (001) surface dominates PbSe growth, and the islands with tilted surfaces grow vertically more slowly. As the misoriented grains are still truncated on {100} planes, their vertical growth rate is limited by the angle these faces make with the growth direction. The coalescence and overgrowth times are affected by the size and distribution of nuclei, which vary considerably within a short range of temperatures and can be difficult to control. This overgrowth is shown by the RHEED patterns in Fig. S1 [34]; immediately after nucleation, diffraction from multiple types of grains is visible, but after continued growth, spots associated with non-(001) grains fade, indicating a smooth single-orientation surface. Similar overgrowth of misoriented grains occurs during growth of the IV-VI SnTe on $SrTiO_3$ [35] where (001) grains are observed to out-grow (111) grains and eventually produce a single-orientation film.

Our observations of misoriented nuclei at low temperatures agree with the observations of Huang *et al.* [21], who grew (110)-oriented PbSe quantum dots on (001) GaSb via LPE. Interestingly, LPE is an equilibrium growth technique but only agrees with the lower-temperature regime we were able to access via MBE. At higher temperatures, we see cube-on-cube nuclei that are mixed with {221} nuclei [effectively (110) nuclei that have tilted over $\pm 19.47°$ for better lattice matching]. Under no condition do we observe single-orientation nucleation on bare III-V substrates. These results highlight the importance of controlling energetic factors beyond lattice-constant matching for successful epitaxy of dissimilar materials. PbSe films grown via MBE on untreated (001)-oriented GaSb, InAs, and GaAs substrates apparently have interfacial energy penalties so high that they are nearly ambivalent to nucleation orientation.

III. CONTROLLED PbSe NUCLEATION VIA SURFACE TREATMENTS

With bare III-V surfaces presenting extremely high interfacial energy penalties and prohibiting single-orientation nucleation, surface treatments were necessary to convert III-As surfaces into better templates for PbSe deposition. In this work, we exposed III-V surfaces to group VI flux and IV-VI molecular flux at high substrate temperature in order to alter the chemistry and symmetry of the surface and achieve single-orientation nucleation. Altering the properties of the growth surface with a brief flux treatment is not a new concept in the growth of dissimilar materials. On III-V substrates, group-V species can be replaced near a film's surface; for example, by exposing GaSb to arsenic flux at elevated temperatures, the top monolayers can be converted to GaAs [36]. In MBE growth of heterovalent ZnSe/GaAs interfaces, a brief pre-exposure to either selenium or zinc flux changes the growth mode significantly [37], with zinc pre-exposure possibly supporting charge neutrality during interface formation [38]. Growing PbSe on III-V substrates, Huang *et al.* [21] hypothesized that selenium could replace antimony near the substrate surface, and Wang *et al.* [25] exposed their GaAs substrates to Te flux during the GaAs oxide desorb before PbSe growth.

Attempts to treat Sb-terminated GaSb (001) with selenium or PbSe flux were markedly unsuccessful. The surface would begin to disorder upon exposure to the flux, as assessed via RHEED (Fig. S2 [34]). Prolonged exposure continued to make the RHEED patterns more diffuse until no structure was visible. These observations, combined with occasional subinterface defects observed by transmission electron microscopy (TEM) (Fig. S3 [34]), point towards reactions occurring at the GaSb/PbSe interface, which degrade the surface and result in low-quality PbSe films. It is worth noting that antimony and selenium have more disparate electronegativities than arsenic and selenium, and Sb_2Se_3 has a lower formation energy than As_2Se_3 [39]. This suggests that Se-Sb interfacial reactions are much more likely.

We find that arsenide surfaces are very receptive to surface treatments towards single-orientation nucleation. Here, InAs provides a useful contrast to GaSb by presenting a chemically different surface on which to nucleate PbSe while retaining a relatively small lattice mismatch. The bare (001) InAs 4×2 reconstruction is shown in Fig. 2, followed by the stages of surface conversion and film growth. To modify the surface for PbSe nucleation, the substrate is brought to 400 °C and exposed to 3×10^{-7} Torr PbSe flux for 10–30 s. At this flux and temperature, PbSe evaporation is faster than deposition, so we observed no multilayer accumulation of PbSe on the surface. During this treatment the growth rate is effectively zero. It appears all unused Se species readily evaporate, and while some lead possibly re-evaporates, the lower vapor pressure of lead sometimes caused lead droplets to form on the surface for long exposures. In the first 5–10 s of PbSe exposure, the 4×2 reconstruction transforms to a well-defined 2×1 reconstruction. If PbSe flux is continued, after 2–4 min, the surface disorders along one axis into an $n \times 1$ reconstruction. Both the 2×1 and the $n \times 1$ reconstructions appear to be robust below 400 °C—the PbSe flux can be halted and either reconstruction will persist while the substrate is cooled to 330 °C before PbSe flux is reinitiated to begin growth. The 2×1 and $n \times 1$ reconstructions can be produced by identical methods from both the InAs 4×2 and the GaAs 2×4 surfaces.

We can now achieve single-orientation (001) nucleation of PbSe on either the 2×1 or the $n \times 1$ treated surface at

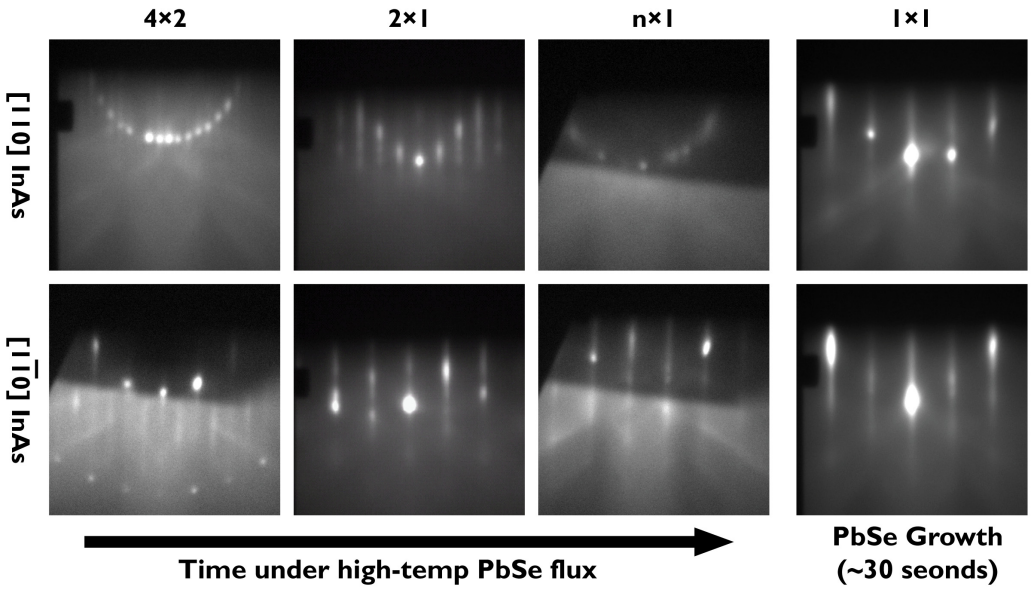

FIG. 2. RHEED patterns showing the evolution of an InAs surface treated with PbSe flux at 400 °C and the subsequent start of PbSe growth at 330 °C. The initial 4 × 2 surface is replaced with a 2 × 1 reconstruction after 5–10 s, and eventually an $n \times 1$ reconstruction after 2–4 min. Both the 2 × 1 reconstruction and the $n \times 1$ reconstruction suppress formation of off-orientation PbSe grains at high temperatures, so at the onset of PbSe growth at 330 °C, a streaky 1 × 1 reconstruction is recovered very quickly. Even when the film has not fully coalesced (see Fig. 5 below), the only 3D diffraction can come from the step edges of otherwise smooth islands.

temperatures greater than ≈310 °C, suppressing all {221}-oriented nuclei that we saw on untreated surfaces at elevated nucleation temperature. The (001)-oriented nuclei exhibit a typical unreconstructed 1 × 1 rocksalt (001) surface during and after growth. We find the growth mode remains Volmer-Weber [three-dimensional (3D) islands and coalescence] and not layer-by-layer, despite this chemical pretreatment. Yet, this conversion of the arsenide surface is able to control nucleation orientation and create a single-orientation film with a sharp interface.

The precise structure of the 2 × 1 and $n \times 1$ reconstructions is not known to us, but we believe that both selenium and lead species are present in the most stable case. Others [40,41] have explored a Se-stabilized 2 × 1 reconstruction on GaAs substrates, but it is unclear if this is the same 2 × 1 reconstruction we observe on PbSe-treated InAs and GaAs. Although we have been able to produce a 2 × 1 reconstruction on InAs using selenium flux only, the process is not as robust as when using PbSe flux, and attempts to control nucleation orientation on InAs using only selenium have been inconsistent. Very high doses of selenium flux on InAs surfaces result in RHEED patterns with chevrons, indicating possible surface reactions and roughening to facets. The presence of lead species may serve to stabilize the new surface structure and prevent deeper reactions from occurring.

IV. INTERFACIAL STRUCTURE AND BONDING

Using high-resolution high-angle annular dark-field (HAADF) STEM, sensitive to atomic number, we have studied the interface formed when PbSe is grown on a PbSe flux-treated 2 × 1 (001) InAs surface. Based on two orthogonal cross-sectional images, we propose a Chain[Pb,As] [42] structure for the hetero-crystal-structure interface, shown in Fig. 3. STEM reveals an As-terminated III-V crystal bonded to a ¼,¼-shifted rocksalt unit cell. Lead atoms take the place of what would be the next layer of indium atoms, apparently bonded to the tetrahedrally coordinated arsenic termination layer. Selenium fills in between the lead to complete the checkerboard (001) rocksalt surface. Lead species effectively continue the indium sublattice, creating a (nominally) continuous cation sublattice across the interface.

The [001] spacing between the top layer of arsenic and the bottom layer of lead is 2.5 Å, intermediate between the $d_{\mathrm{PbSe}(002)} = 3.06$ Å, and $d_{\mathrm{InAs}(004)} = 1.52$ Å. Interestingly, the first few monolayers of PbSe seem slightly distorted, with selenium species slightly displaced away from the interface. The first layer of the selenium sublattice is 0.5 Å displaced from the first layer of the lead sublattice, and this discrepancy fades significantly over the first ∼10 monolayers until the lead and selenium sublattices begin to line up. Figure 4 shows this distortion with two adjacent HAADF-contrast traces across the PbSe/InAs interface.

We hypothesize an interfacial bonding arrangement where the strong covalent bonds from the substrate, a continuation of the tetrahedral bonding from the terminating arsenic layer, extend up to the lead atoms in the first monolayer of IV-VI rocksalt. Obeying more typical IV-VI bonding, the selenium sublattice effectively fills in square interstices in the first monolayer of semitetrahedrally bonded lead. Unlike in bulk rocksalt material, the first layers in the selenium sublattice are compressed (see Fig. 4 inset). This is a different distortion than the alternating rumpling previously seen at PbSe interfaces and surfaces [43,44]. We speculate that charge at the

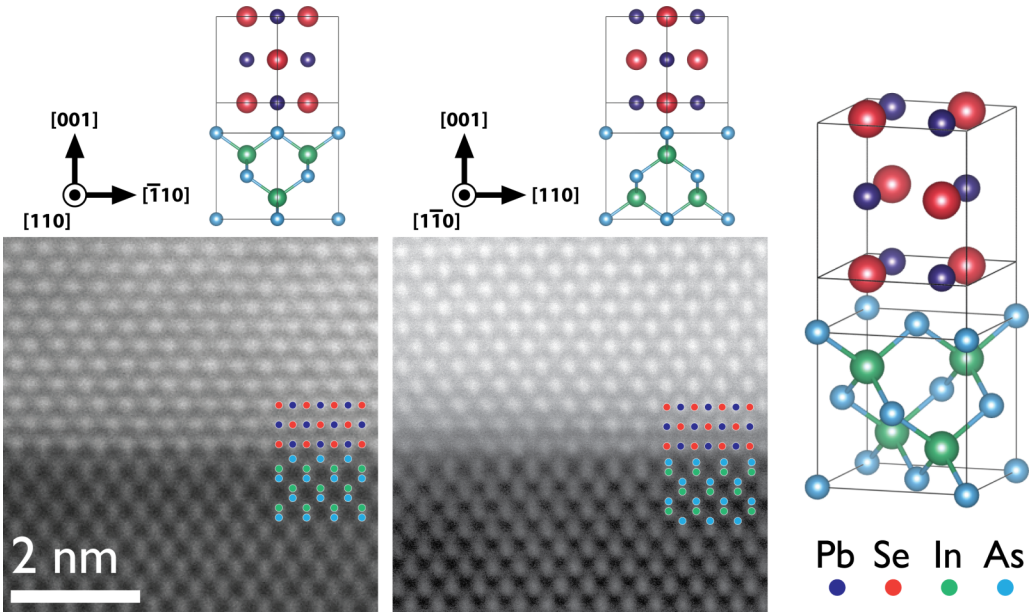

FIG. 3. Cross sectional HADDF-STEM micrographs of the PbSe/InAs interface: The interface is sharp, with no obvious reactions or atomic exchange across the interface. A proposed atomic column mapping/structure is overlaid and shown graphically to the right.

heterovalent interface may be responsible for this spatially varying structural distortion, but more study is required to locate the excess charge that will depend on the band offset between PbSe and InAs, which is not yet known.

If the directional Pb-As bond is critical to the Chain[Pb,As] interface formation, that implies lead is the most important species and is likely present in the most stable 2×1 reconstruction prior to film growth. The variability in PbSe growth on Se-flux treated surface reconstructions may stem from the need for the surface to rapidly rearrange during the onset of deposition. Alternately, a different chain or shadow structure may form on Se-only reconstructed surfaces, but with a lower energy barrier to misorientation. We are currently investigating this.

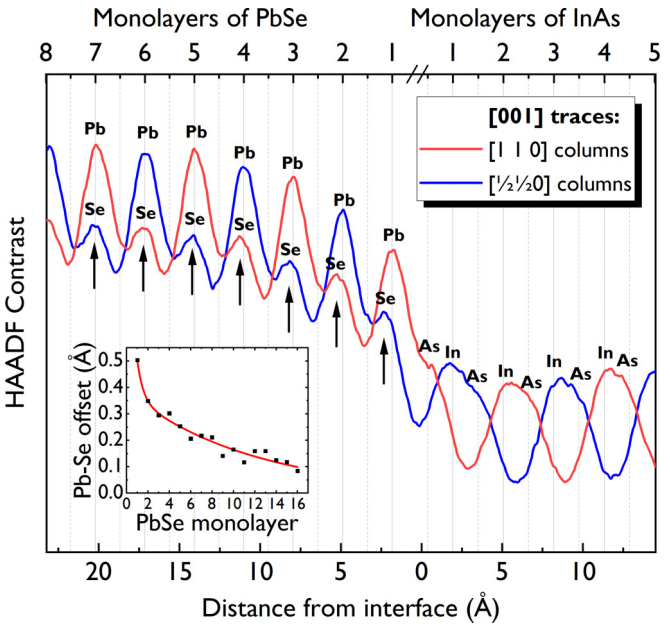

FIG. 4. [001] contrast traces (averaged without fitting) across the HAADF STEM micrograph from Fig. 3 (left). The InAs barbells can be seen on the right, and the alternating Pb/Se species on the left. At the interface, the final InAs layers appear slightly stretched, and the first few monolayers of the selenium sublattice are warped away from the interface. The vertical grid lines are at a regular interval.

This Chain[Pb,As] structure revealed by STEM is unique in its own right. Most studies of heteroepitaxial systems depend on a continuous sublattice of one species. (001) ErAs/GaAs has a continuous FCC arsenic sublattice [45], and both (110) and (001) PbTe/CdTe have a continuous tellurium sublattice [43]. The PbSe/InAs system has no common species between the substrate and film. Unlike these examples with a continuous, same-atom cation sublattice, the PbSe/InAs interface has a mixed-species, continuous-anion sublattice across the interface. Ignoring the interfacial spacing change, the FCC indium sublattice in the substrate matches up with the lead FCC sublattice in the film. As mentioned above, the selenium sublattice in the film seems to have to work around this well-defined lead structure. The theoretical work of Tarnow *et al.* [42] points to either Shadow[As,As] or Chain[Er,As] as the lowest-energy arrangement between As-terminated AlAs and ErAs, or Shadow[As,Al] between Al-terminated AlAs and ErAs. In experiment, Klenev *et al.* [45] observed a Chain[As,In/Ga] structure between InGaAs and ErAs. Although the valency mismatch is different between this system and our IV-VI/III-V growth, our observation of Chain[Pb,As] is most similar to the Chain[Er,As] model, suggesting that the interface could be a thermodynamically optimal one. Experimentally, this hypothesis is supported by the high substrate temperature during the surface treatment, which likely provides sufficient energy for the surface to exit any local minimum arrangement, preparing for growth of a thermodynamically optimal interface.

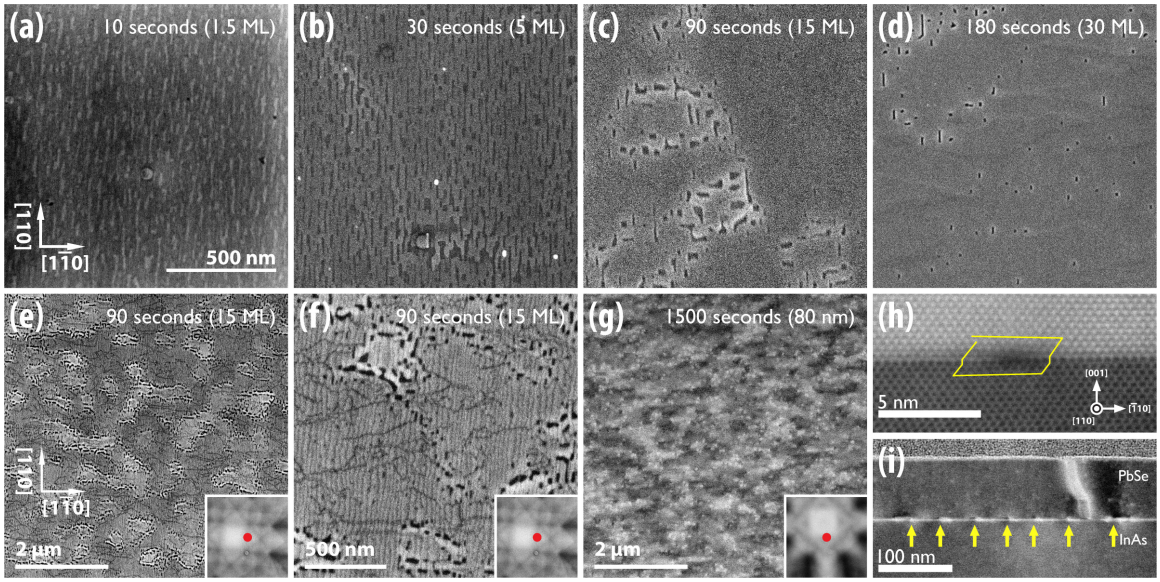

FIG. 5. Coalescence of PbSe islands on InAs (a)–(d) SEM micrographs of PbSe coalescence geometry: After nucleation on the 2 × 1 InAs surface, initial elongated islands come together to form a dense network. As this is "filled in" by continued PbSe flux, some gaps remain, decorating the edges of low-angle grain boundaries. Eventually the film fully coalesces, resulting in a moderately smooth, hole-free surface. (e-i) Origin and persistence of coalescence defects: (e),(f) ECCI micrographs ({220} conditions) of a coalescing 90-s growth with orientation contrast highlighting low angle grain boundaries bordered by holes in the film. (g) ECCI micrograph of a fully coalesced film highlighting the persistence of these slight misorientations, now decorated by threading dislocations. (h),(i) HR-HAADF STEM and DFSTEM of the PbSe/InAs interface, looking down the [110] zone axis. In ECCI (f), dark lines within grains form a grid of dislocations highly ordered across [1$\bar{1}$0] but inconsistent across [110]; these misfits are also observed in STEM; and a single misfit from the PbSe/InAs interface is traced with an incomplete Burgers circuit. We also believe the prominent planar defect in the DFSTEM micrograph is a low angle grain boundary like those visible in ECCI.

V. PbSe COALESCENCE AND FILM STRUCTURE

In order to examine the continued growth behavior of single-orientation PbSe towards usable thin films, we truncated growth at different stages of island coalescence and characterized the structure with standard secondary electron imaging as well as electron channeling contrast imaging (ECCI) in SEM. Diffraction-contrast and HAADF STEM were used to examine defects in coalesced films.

The SEM of partially coalesced samples grown at 330 °C (Fig. 5) reveals the single-orientation (001) PbSe islands that form on the treated 2 × 1 (001) InAs surface are significantly longer in the [110] direction and very shallow in the [001] (growth) direction. Although they rapidly form an interconnected network, they are slow to coalesce into a smooth pinhole-free film. At these growth temperatures, the sticking coefficient of PbSe on the treated InAs surface is near unity, with rapid PbSe migration across the surface enabling the formation of few-monolayer-tall islands (see Fig. S4 [34] for detail on island height). Figures 5(a)–5(d) shows the coalescence progression of PbSe films on InAs. After only ≈1.5 monolayers (ML) of PbSe flux, (001)-oriented islands begin to elongate in the [110] direction. After 5 ML of deposition, these islands are fully interconnected, and after 15 ML, there are large regions of flat coalesced film developing. The remaining gaps in the film coalesce slowly, forming defects which decorate low-angle grain boundaries in the coalesced film.

After 5 min (∼15 nm) of growth at 330 °C nucleation temperature, the films are generally fully coalesced, but the best results were obtained by subsequently dropping the temperature by 30–60 °C and continuing growth at a lower temperature. These two-temperature growths produced the highest quality fringing in XRD, and produced 80-nm films with an atomic force microscopy-measured RMS roughness of 1.8 nm over a 2 × 2 μm area.

The elongation of the initial nuclei shapes is likely inherited from the dimerized 2 × 1 PbSe:InAs surface. As adjacent islands grow together, they create a grid of dislocations, very closely spaced in the [1$\bar{1}$0] direction, but more irregular and spread-out in the [110] direction. Figures 5(e) and 5(f) show orientation-sensitive ECCI micrographs of the grain structure of these films during and after coalescence. The resultant grains are slightly elongated in the [1$\bar{1}$0] direction, and the dislocation density necessary to define these small grains is very high.

Figure 5(h) and 5(i) show a more detailed view of one these boundaries and an array of misfit dislocations. Low-angle grain boundaries appear inconsistently every few hundred nanometers, while the misfit dislocations are evenly spread along the interface, remnants of island coalescence. The Burgers circuit traced in Fig. 5(h) indicates a Burgers vector of $\frac{1}{2}$[101] or $\frac{1}{2}$[0$\bar{1}$1]; with a line direction of [110], these dislocations must be sessile, unable to rearrange at the interface to form an even grid as has been observed at PbTe/PbSe interfaces [46]. The less-regular [1$\bar{1}$0]-oriented

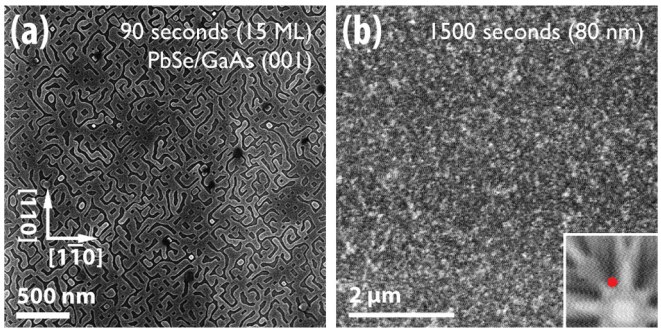

FIG. 6. Coalescence of PbSe islands on GaAs. (a) SEM micrograph of a coalescing PbSe layer on GaAs. The islands have formed an interconnected network but have not fully coalesced into a smooth film. The islands preferentially truncate on {100} planes. (b) ECCI micrograph of a fully coalesced film. Orientation contrast highlights the high density and uniformity of low-angle grain boundaries.

dislocations observed in Fig. 5(f) are likely similar and also locked-in immediately after island coalescence. Although the primary {100}⟨110⟩ slip system in PbSe is active even at low temperatures, dislocations in this system experience no resolved shear stress from in-plane biaxial strain for (001)-oriented growth [47], preventing glide of any dislocations to alleviate film-substrate mismatch.

On InAs, we hypothesized that the holes visible early in PbSe film growth could be the result of local strain between islands as a result of lattice mismatch, where holes encapsulated nonzero Burgers circuits. Growth on the chemically similar but significantly lattice-mismatched (001) GaAs surface gives us the opportunity to examine this in more detail. (001) PbSe islands on treated (001) GaAs surfaces favor termination on {100}-type planes—the low-energy-rocksalt planes [Fig. 6(a)]—rather than elongating in the [110] direction as on treated InAs [Fig. 5(a)] or having little lateral order as on GaSb [Figs. 1(e) and 1(f)]. It appears that connected PbSe islands on GaAs grow laterally to a characteristic width of 40–50 nm then grow vertically, leaving a notable fraction of exposed substrate even after significant material deposition. Compared to an equivalent growth on InAs [Fig. 5(c)], the coalescence on GaAs (Fig. 6) is extremely slow, suggesting PbSe adatoms may have higher mobility around highly strained crystals.

Coalesced PbSe films grown on InAs substrates are of relatively high crystalline quality with sharp interfaces, good rocking curve widths, and good registry to the substrate (Fig. 7). The 2θ-ω full width at half maximum (FWHM) of the PbSe (004) peak is 410 arcsec for an 80-nm film, and for a thicker ∼320-nm film, a 2θ-ω FWHM of just 181 arcsec was measured. For the 80-nm film, mosaic twist about the [001] direction was measured via a {224} ω rocking curve in skew-symmetric geometry, with an observed FWHM of 457 arcsec. Mosaic tilt in the 80-nm film was measured with orthogonal (004) ω rocking curves. FWHMs of 185 and 369 arcsec were observed about the [110] and [1$\bar{1}$0] directions, respectively. This result is on par with μm-thick layers of PbSe on (001) GaAs, with a rocking curve FWHM of 266 arcsec reported by Wang *et al.* [25]. Figure 7 also includes a pole figure, a 360° ϕ-scan of the {224} peaks of PbSe and InAs, showing excellent epitaxial registry with no apparent population of significantly twisted grains. Analysis of ECCI micrographs [Fig. 5(g)] yields a threading dislocation density in the mid 10^9 cm^{-2}.

Coalesced films of PbSe on InAs contain residual strain resulting from asymmetric relaxation that slightly distorts the cubic lattice. This residual strain is a combination of lattice mismatch during growth and thermal mismatch during cooldown. Measurements of the {224} plane spacing reveals that the PbSe unit cell at room temperature is 0.02% compressed along the [1$\bar{1}$0] direction and 0.2% stretched along the [110] direction. We believe this asymmetric relaxation is due to the asymmetric distribution of dislocations observed in ECCI during the early stages of growth [Fig. 5(f)], affecting relaxation both at growth temperature and during cooldown. Even with a significant difference in the misfit density in

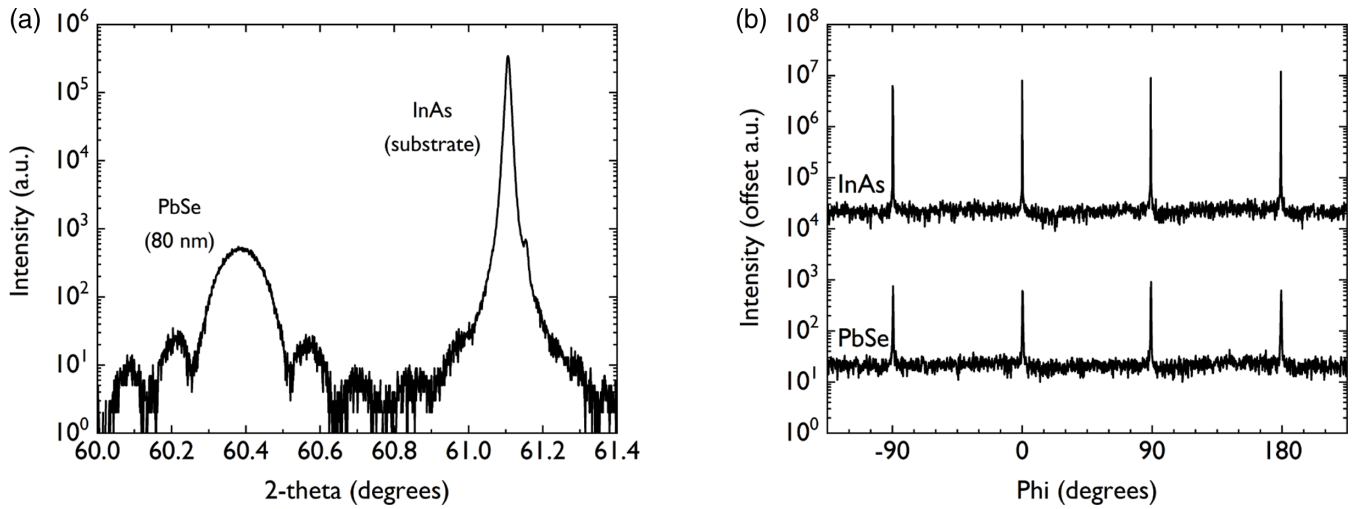

FIG. 7. Crystallinity of PbSe films on InAs: (a) 2θ-ω coupled scan of the (004) peak showing a high-quality interface with distinct thickness fringes. (b) A 360° ϕ-scan of the {224} peaks in PbSe and InAs, showing that the nominal epitaxial registration between the film and substrate is (001) cube-on-cube.

orthogonal directions, the relaxation of in-plane strain is hindered by the immobility of PbSe's primary slip system in the (001) orientation.

VI. DISCUSSION

Unsurprisingly, the IV-VI rocksalts are not known to grow layer-by-layer on any non-IV-VI surface. The high interfacial energy of heteronucleation prevents otherwise low-surface-energy rocksalt films from wetting the relatively high-energy surfaces of fluorite [29,48,49], diamond cubic [29,50], cubic perovskite [35], or zincblende [21,25,26] substrates. Poor bonding between ionic PbSe and covalent Si has also been known to prevent growth of high quality layers [29], and weak bonding between IV-VI films and BaF_2 substrates has also been observed.

The well-controlled PbSe nucleation we have been able to achieve in this work likely depends on a crucial first layer structure. We believe we are close to a thermodynamically stable interface, where the high-temperature PbSe surface treatment gives this first interfacial layer sufficient time to anneal into a favorable arrangement. As PbSe readily evaporates at treatment temperatures, it is likely the impingent PbSe species can only adhere if in an extremely stable low-energy configuration with relatively strong bonds to the substrate. Any PbSe that does not have a direct and stable connection with the top layer of substrate is quickly desorbed. Unfortunately, the associated decrease in the interfacial energy penalty with this ordering is not severe enough to allow for layer-by-layer growth, merely oriented Volmer-Weber growth. That said, the island shape and coalescence behavior of PbSe on (001) InAs implies significant interaction between the film and substrate. This interaction is also tunable; the shape of PbSe islands on the more lattice-mismatched yet chemically similar (001) GaAs surface is dictated by low-energy IV-VI facets and inherits no symmetry from the III-V surface they bond to.

For certain compositions, IV-VI materials such as SnTe and PbSnSe exhibit a TCI phase with an inverted bandgap. Such a state is linked to crystal mirror symmetries, so tracking symmetry across the heterovalent interface is important for considering future applications. The 2×1 reconstruction appears to leave behind no residual disorder or partial monolayers at the interface so the nominal atomic structure we observe at the IV-VI/III-V interface is a near best-case scenario for preserving symmetry: one crystal structure simply ends and the other begins. That said, there are two structural distortions present near the interface with potentially interesting effects. The asymmetric strain state resulting from island coalescence imposes a shear in the (001) plane, which maintains important mirror symmetries, but still distorts the band structure and has been predicted [51] to shift but not gap topological states on the (001) rocksalt surface. The other significant symmetry-altering perturbation at the interface is the offset between the Pb and Se sublattices very near the III-V termination. Serbyn and Fu [51] show that the rhombohedral ferroelectric distortion ($w = \langle 110 \rangle$) breaks one mirror symmetry and gaps the topological surface states. If the ($w = [001]$) distortion we observe has similar behavior it may gap the states immediately at the interface, but because this distortion is isolated close to the heterointerface, it should displace the topological interface state deeper into the IV-VI film.

The results we discuss in this paper illuminate important features of film nucleation and growth in this significantly mismatched heteroepitaxial system, highlighting surface chemistry as a defining factor for film nucleation orientation and lattice mismatch as a defining factor for early nuclei shape and behavior, together building towards effective IV-VI/III-V heterostructures for infrared and topological device applications. Future work can explore the chemistry-dependent nucleation of PbSe on other III-V surfaces, notably the (111) surface where dislocation glide is possible. Many of the same kinetic arguments may apply, despite a geometrically different interface. It may also be possible to control band offset if a different surface treatment can produce a different interfacial structure at an (001) interface then the Chain[Pb,As] structure we observed here. Perfectly abrupt heterovalent interfaces are thermodynamically unstable; change in growth conditions might lead to a variability in the degree of atomic intermixing and impact the band offset and doping in the film. Further studies on PbSe coalescence behavior have two promising avenues: reducing the number of coalescence defects by removing the lattice mismatch altogether using ternary III-V surfaces or eliminating defects during growth via thermal cycling in an appropriately oriented film.

VII. EXPERIMENTAL

All PbSe films were grown in a Riber Compact 21T MBE system utilizing a compound PbSe source. PbSe flux was measured by a beam flux gauge at approximately 3×10^{-7} Torr for all growths. GaSb buffer layers utilized a conventional gallium effusion cell, and a valved cracker cell for antimony. Selenium surface treatments were also provided with a valved cracker source operating at 500 °C.

GaSb surfaces were prepared by desorbing the oxide layer from epiready wafers under antimony flux and growing 150 nm of GaSb to produce an atomically smooth surface. GaSb substrate surface temperature was measured via offset from the $2 \times 5/1 \times 3$ surface reconstruction phase transition of GaSb at a measured antimony flux of 1×10^{-7} Torr. The temperature offset was measured by thermocouple and was sometimes inconsistent from sample to sample based on mounting. Reported temperatures above are closest approximations of the real temperature based on later pyrometry measurements.

InAs and GaAs substrates were similarly prepared for growth in a separate MBE chamber, including oxide desorb and growth of a thin homoepitaxial layer for improved surface smoothness. Use of two separate MBE systems necessitated capping prepared substrates with amorphous arsenic to protect the surface during nonvacuum transfer to the IV-VI system. InAs and GaAs surface temperature was measured via pyrometer.

With our temperature calibrations, growth rate was constant under 340–350 °C, and films did not grow above 360–370 °C. The best growths were above 325 °C to extinguish the misoriented grains, but below 345 °C to avoid PbSe evaporation from the surface and subsequent roughening. The 80-nm thickness samples analyzed in Figs. 3, 4, 5(g)–5(i),

6(b), and 7 were grown to coalescence at 330 °C and grown to full thickness at 270 °C.

RHEED patterns were recorded *in situ* during MBE growth, utilizing a 15kV incident beam; SEM micrographs were taken using an FEI Nova Nano 650 SEM in immersion mode; ECCI micrographs were taken utilizing an FEI Quanta 400 SEM using a high-angle backscatter detector and a 30-kV incident beam with channeling contrast produced by the (220) condition; and STEM micrographs were recorded on an FEI Talos STEM utilizing HAADF and ADF detectors. All images shown here have only been processed with linear contrast/brightness adjustments.

ACKNOWLEDGMENTS

This work was supported by the National Science Foundation (NSF) through the Materials Research Science and Engineering Center (MRSEC) Program through Grant No. DMR 1720256 (Seed). B.B.H. acknowledges support from the National Science Foundation (NSF) Graduate Research Fellowship under Grant No. 1650114. We thank D. Jung for providing regrown InAs substrates, C. Reilly for x-ray diffractometry analysis, and C. Palmstrøm and J. Speck for useful discussions. We also would like to acknowledge K. Olsson and J. English for their MBE expertise and support.

[1] C. J. Palmstrom, Epitaxy of dissimilar materials, Annu. Rev. Mater. Sci. **25**, 389 (1995).

[2] R. Nicolini, L. Vanzetti, G. Mula, G. Bratina, L. Sorba, A. Franciosi, M. Peressi, S. Baroni, R. Resta, A. Baldereschi, J. E. Angelo, and W. W. Gerberich, Local Interface Composition and Band Discontinuities in Heterovalent Heterostructures, Phys. Rev. Lett. **72**, 294 (1994).

[3] M. Sukhotin, E. R. Brown, A. C. Gossard, D. Driscoll, M. Hanson, P. Maker, and R. Muller, Photomixing and photoconductor measurements on ErAs/InGaAs at 1.55 μm, Appl. Phys. Lett. **82**, 3116 (2003).

[4] J. M. Zide, D. O. Klenov, S. Stemmer, A. C. Gossard, G. Zeng, J. E. Bowers, D. Vashaee, and A. Shakouri, Thermoelectric power factor in semiconductors with buried epitaxial semimetallic nanoparticles, Appl. Phys. Lett. **87**, 112102 (2005).

[5] W. Kim, J. Zide, A. Gossard, D. Klenov, S. Stemmer, A. Shakouri, and A. Majumdar, Thermal Conductivity Reduction and Thermoelectric Figure of Merit Increase by Embedding Nanoparticles in Crystalline Semiconductors, Phys. Rev. Lett. **96**, 045901 (2006).

[6] H. Zogg, K. Kellermann, K. Alchalabi, and D. Zimin, Optically pumped lead-chalcogenide mid-infrared emitters on silicon substrates, Infrared Phys. Technol. **46**, 155 (2004).

[7] P. J. McCann, I. Chao, H. Sachar, D. McAlister, C. Li, X. Fang, H. Wu, and K. Namjou, IV–VI Semiconductor growth on silicon substrates and new mid-infrared laser fabrication methods, Spectrochim. Acta Part A Mol. Biomol. Spectrosc. **55**, 1999 (1999).

[8] L. A. Elizondo, Y. Li, A. Sow, R. Kamana, H. Z. Wu, S. Mukherjee, F. Zhao, Z. Shi, and P. J. McCann, Optically pumped mid-infrared light emitter on silicon, J. Appl. Phys. **101**, 104504 (2007).

[9] H. Zogg, K. Alchalabi, and D. Zimin, Lead chalcogenide on silicon infrared focal plane arrays for thermal imaging (Review Paper), Def. Sci. J. **51**, 53 (2001).

[10] H. Zogg, K. Alchalabi, D. Zimin, K. Kellermann, and W. Buttler, Two-dimensional monolithic lead chalcogenide infrared sensor array on silicon read-out chip, Nucl. Instrum. Methods Phys. Res., Sect. A **512**, 440 (2003).

[11] W. Heiss, T. Schwarzl, G. Springholz, K. Biermann, and K. Reimann, Above-room-temperature mid-infrared lasing from vertical-cavity surface-emitting PbTe quantum-well lasers, Appl. Phys. Lett. **78**, 862 (2001).

[12] M. Eibelhuber, T. Schwarzl, G. Springholz, and W. Heiss, Lead salt microdisk lasers operating in continuous wave mode at 5.3 μm wavelength, Appl. Phys. Lett. **94**, 021118 (2009).

[13] G. Springholz and G. Bauer, Semiconductors, IV-VI, in *Wiley Encyclopedia of Electrical and Electronics Engineering* (Wiley, Hoboken, NJ, 2014), pp. 1–16.

[14] P. Dziawa, B. J. Kowalski, K. Dybko, R. Buczko, A. Szczerbakow, M. Szot, E. Łusakowska, T. Balasubramanian, B. M. Wojek, M. H. Berntsen, O. Tjernberg, and T. Story, Topological crystalline insulator states in $Pb_{1-x}Sn_xSe$, Nat. Mater. **11**, 1023 (2012).

[15] E. O. Wrasse and T. M. Schmidt, Prediction of two-dimensional topological crystalline insulator in PbSe monolayer, Nano Lett. **14**, 5717 (2014).

[16] J. Liu, W. Duan, and L. Fu, Two types of surface states in topological crystalline insulators, Phys. Rev. B **88**, 241303 (2013).

[17] Y. Tanaka, Z. Ren, T. Sato, K. Nakayama, S. Souma, T. Takahashi, K. Segawa, and Y. Ando, Experimental realization of a topological crystalline insulator in SnTe, Nat. Phys. **8**, 800 (2012).

[18] T. H. Hsieh, H. Lin, J. Liu, W. Duan, A. Bansil, and L. Fu, Topological crystalline insulators in the SnTe material class, Nat. Commun. **3**, 982 (2012).

[19] Z. Wang, Q. Liu, J.-W. Luo, and A. Zunger, Digging for topological property in disordered alloys: The emergence of Weyl semimetal phase and sequential band inversions in PbSe–SnSe alloys, Mater. Horizons **6**, 2124 (2019).

[20] Z. Shi, GaSb–PbSe–GaSb double heterostructure midinfrared lasers, Appl. Phys. Lett. **72**, 1272 (1998).

[21] X. L. Huang, Z. Labadi, A. Hammiche, and A. Krier, Growth of self-assembled PbSe quantum-dots on GaSb (100) by liquid phase epitaxy, J. Phys. D **35**, 3091 (2002).

[22] R. Yoshimi, A. Tsukazaki, K. Kikutake, J. G. Checkelsky, K. S. Takahashi, M. Kawasaki, and Y. Tokura, Dirac electron states formed at the heterointerface between a topological insulator and a conventional semiconductor, Nat. Mater. **13**, 253 (2014).

[23] J. Raty, M. Schumacher, P. Golub, V. L. Deringer, C. Gatti, and M. Wuttig, A quantum-mechanical map for bonding and properties in solids, Adv. Mater. **31**, 1806280 (2019).

[24] G. Lucovsky and R. M. White, Effects of resonance bonding on the properties of crystalline and amorphous semiconductors, Phys. Rev. B **8**, 660 (1973).

[25] X. J. Wang, Y. B. Hou, Y. Chang, C. R. Becker, R. F. Klie, T. W. Kang, R. Sporken, and S. Sivananthan, Heteroepitaxy of PbSe on GaAs(100) and GaAs(211)B by molecular beam epitaxy, J. Cryst. Growth **311**, 2359 (2009).

[26] H. Clemens, H. Krenn, B. Tranta, P. Ofner, and G. Bauer, Epitaxial growth of PbTe on (111)BaF_2 and (100)GaAs, Superlattices Microstruct. **4**, 591(1988).

[27] J. Yoshino, Growth of PbTe/CdTe on GaAs (100), J. Vac. Sci. Technol. B **5**, 683 (1987).

[28] W. Wang, G. Lee, M. Huang, R. M. Wallace, and K. Cho, First-principles study of GaAs(001)-$\beta 2(2 \times 4)$ surface oxidation and passivation with H, Cl, S, F, and GaO, J. Appl. Phys. **107**, 103720 (2010).

[29] P. Müller, A. Fach, J. John, A. N. Tiwari, H. Zogg, and G. Kostorz, Structure of epitaxial PbSe grown on Si(111) and Si(100) without a fluoride buffer layer, J. Appl. Phys. **79**, 1911 (1996).

[30] M. R. Jordan and D. J. Stirland, Changes in epitaxy produced by electron bombardment, Thin Solid Films. **8**, 221 (1971).

[31] G. Springholz, Molecular Beam Epitaxy of IV-VI Heterostructures and Superlattices, in *Lead Chalcogenides: Physics and Applications*, edited by D. Khokhlov (Taylor and Francis, New York, 2003), pp. 123–207.

[32] H. Holloway, E. M. Logothetis, and E. Wilkes, Epitaxial growth of lead tin telluride, J. Appl. Phys. **41**, 3543 (1970).

[33] D. K. Hohnke and S. W. Kaiser, Epitaxial PbSe and $Pb_{1-x}Sn_x$ Se: Growth and electrical properties, J. Appl. Phys. **45**, 892 (1974).

[34] See Supplemental Material at http://link.aps.org/supplemental/10.1103/PhysRevMaterials.4.033402 for more details.

[35] O. E. Dagdeviren, C. Zhou, K. Zou, G. H. Simon, S. D. Albright, S. Mandal, M. D. Morales-Acosta, X. Zhu, S. Ismail-Beigi, F. J. Walker, C. H. Ahn, U. D. Schwarz, and E. I. Altman, Length scale and dimensionality of defects in epitaxial SnTe topological crystalline insulator films, Adv. Mater. Interfaces **4**, 1601011 (2017).

[36] R. Kaspi, J. Steinshnider, M. Weimer, C. Moeller, and A. Ongstad, As-soak control of the InAs-on-GaSb interface, J. Cryst. Growth **225**, 544 (2001).

[37] S. Guha, H. Munekata, and L. L. Chang, Structural quality and the growth mode in epitaxial ZnSe/GaAs(100), J. Appl. Phys. **73**, 2294 (1993).

[38] S. Miwa, L. H. Kuo, K. Kimura, T. Yasuda, A. Ohtake, C. G. Jin, and T. Yao, The role of zinc pre-exposure in low-defect ZnSe growth on As-stabilized GaAs (001), Appl. Phys. Lett. **73**, 939 (1998).

[39] A. Jain, S. P. Ong, G. Hautier, W. Chen, W. D. Richards, S. Dacek, S. Cholia, D. Gunter, D. Skinner, G. Ceder, and K. A. Persson, Commentary: The Materials Project: A materials genome approach to accelerating materials innovation, APL Mater. **1**, 011002 (2013).

[40] S. Takatani, T. Kikawa, and M. Nakazawa, Reflection high-energy electron-diffraction and photoemission spectroscopy study of GaAs(001) surface modified by Se adsorption, Phys. Rev. B **45**, 8498 (1992).

[41] D. Li and M. D. Pashley, ZnSe nucleation on the GaAs(001):Se-(2×1) surface observed by scanning tunneling microscopy, J. Vac. Sci. Technol. B **12**, 2547 (1994).

[42] E. Tarnow, Structure of the interface between ErAs, a cubic semimetal and AlAs, a tetrahedral semiconductor, J. Appl. Phys. **77**, 6317 (1995).

[43] R. Leitsmann, L. E. Ramos, F. Bechstedt, H. Groiss, F. Schäffler, W. Heiss, K. Koike, H. Harada, and M. Yano, Rebonding at coherent interfaces between rocksalt-PbTe/zinc-blende-CdTe, New J. Phys. **8**, 317 (2006).

[44] J. Ma, Y. Jia, Y. Song, E. Liang, L. Wu, F. Wang, X. Wang, and X. Hu, The geometric and electronic properties of the PbS, PbSe and PbTe (001) surfaces, Surf. Sci. **551**, 91 (2004).

[45] D. O. Klenov, J. M. Zide, J. D. Zimmerman, A. C. Gossard, and S. Stemmer, Interface atomic structure of epitaxial ErAs layers on (001) $In_{0.53}Ga_{0.47}As$ and GaAs, Appl. Phys. Lett. **86**, 241901 (2005).

[46] G. Springholz and K. Wiesauer, Nanoscale Dislocation Patterning in PbTe/PbSe(001) Lattice-Mismatched Heteroepitaxy, Phys. Rev. Lett. **88**, 015507 (2001).

[47] P. Müller, H. Zogg, A. Fach, J. John, C. Paglino, A. N. Tiwari, M. Krejci, and G. Kostorz, Reduction of Threading Dislocation Densities in Heavily Lattice Mismatched PbSe on Si(111) by Glide, Phys. Rev. Lett. **78**, 3007 (1997).

[48] J. Stoemenos, N. N. Zheleva, and M. H. Koparanova, Structural study of PbTe films grown on BaF_2 by hot wall epitaxy, J. Cryst. Growth **97**, 443 (1989).

[49] P. Pongratz and H. Sitter, TEM analysis of lead telluride films grown by hot-wall epitaxy on KCI and BaF_2, J. Cryst. Growth **80**, 73 (1987).

[50] H. Zogg, P. Mueller, A. Fach, J. John, C. Paglino, and A. N. Tiwari, Epitaxy of narrow gap IV-VI materials on Si(111) and Si(100) substrates: Growth, properties, and thermal mismatch strain accommodation, in *SPIE's 1995 International Symposium on Optical Science, Engineering, and Instrumentation*, edited by R. E. Longshore, J. W. Baars, A. Kepten, and J. M. Trombetta (SPIE, Bellingham, WA, 1995), pp. 35–42.

[51] M. Serbyn and L. Fu, Symmetry breaking and Landau quantization in topological crystalline insulators, Phys. Rev. B **90**, 035402 (2014).